


For Reference

NOT TO BE TAKEN FROM THIS ROOM

Ex LIBRIS
UNIVERSITATIS
ALBERTAENSIS





Digitized by the Internet Archive
in 2023 with funding from
University of Alberta Library

<https://archive.org/details/Mozeson1974>

THE UNIVERSITY OF ALBERTA
FATIGUE CRACK PROPAGATION IN LINE PIPE STEEL WELDMENTS

by



CHARLES EDWARD MOZESON

A THESIS

SUBMITTED TO THE FACULTY OF GRADUATE STUDIES AND RESEARCH
IN PARTIAL FULFILMENT OF THE REQUIREMENTS FOR THE DEGREE

OF MASTER OF SCIENCE
IN METALLURGICAL ENGINEERING

DEPARTMENT OF MINERAL ENGINEERING

EDMONTON, ALBERTA

SPRING, 1974

ABSTRACT

The effect of temperature upon fatigue crack propagation in a fine-grained, API 5LS -- X-65 steel, a simulated heat-affected zone, and a double-V submerged arc weldment were investigated. Constant deflection bending fatigue tests at 640 cpm were conducted on single-edge, keyhole notched specimens in prepurified, dried argon gas. Nominal temperatures of testing were -45C, -10C, 21C, and 77C.

In addition to fatigue testing, tensile tests were performed at 0.01 in/minute. Strain-ageing tests were also conducted by ageing for one hour at -18C, 24C, 100C, or 204C, under either tensile loading (0.10 in/minute) or fatigue cycling (2.5 cpm) at pulsating stress equivalent to the prior flow stress ($R = 0$).

The plane strain fatigue data were analyzed according to the fracture mechanics relationship $da/dN = C (\Delta K)^m$, where da/dN is the crack propagation rate, ΔK is the range of stress-intensity.

In general, the decrease in yield strength with temperature causes an increase in da/dN for a given ΔK . However, an increase in the yield strength -- probably due to strain-ageing -- causes a decrease in da/dN for all three metal structures studied in the region of -7C to 32C. Above 32C, overageing may have occurred, resulting in an increased crack propagation rate.

The weld metal was determined to be the most resistant to fatigue crack propagation, followed by the heat-affected zone, and the base metal.

ACKNOWLEDGEMENTS

I wish to express my sincere thanks to Dr. F. H. Vitovec for suggesting and supervising this research topic and for his untiring assistance throughout the project.

I am grateful to Mr. R. M. Scott, Mr. T. Forman, Mr. R. Konzuk, Mr. B. Snider, and Mr. G. Chiasson, for their technical assistance.

I am indebted to Dr. M. L. Wayman for his advice and discussions that helped forward the progress of this research.

The Interprovincial Steel and Pipe Corporation, Limited, is hereby acknowledged for supplying the sample material used in this project.

I would like to thank my wife, Laurie, for her extreme patience and understanding during the period of this research.

This project was supported by the National Research Council of Canada under Grant number A2926.

TABLE OF CONTENTS

	Page
Chapter 1. INTRODUCTION	1
Chapter 2. EXPERIMENTAL PROCEDURE	4
2.1. Introduction	4
2.2. Test Material	4
2.3. Microstructure	5
2.4. Heat Treatment	5
2.5. Fatigue Test Specimen Preparation	6
2.6. Static and Dynamic Tensile Tests	6
2.7. Calculation of Stress-intensity Factor	7
2.8. Testing Machine and Fatigue Testing Procedure	8
Chapter 3. EXPERIMENTAL RESULTS	10
3.1. Crack Length versus Number of Fatigue Cycles	10
3.2. Crack Growth Rate versus ΔK	10
Chapter 4. ANALYSIS AND DISCUSSION	13
Chapter 5. SUMMARY AND CONCLUSIONS	21
TABLES	23
FIGURES	26
BIBLIOGRAPHY	54

LIST OF TABLES

TABLE		Page
I	Chemical composition and mechanical properties of base metal and weld metal	24
II	Tested tensile properties of base metal	25

LIST OF ILLUSTRATIONS

FIGURE		Page
1	Microstructure of the as-received base material (X500)	27
2	Preferred grain orientation and banding in base metal (X100)	28
3	Nonmetallic inclusions of the base metal (X100)	29
4	Macrostructure of the weld (X5)	30
5	Microstructure of the simulated heat-affected zone (X500)	31
6	Microstructure of the grain-coarsened H.A.Z. of the weld (X500)	32
7	Cooling curve of the induction-heated, simulated H.A.Z.	33
8	Schematic illustration of the fatigue testing machine (after Andreasen, 1973)	35
9	Fatigue testing machine, showing specimen orientation	36
10	Crack length versus fatigue cycles, for welded samples	37
11	da/dN versus ΔK for the base metal at 21C	38
12	da/dN versus ΔK for the base metal at -48C and -7C	39
13	da/dN versus ΔK for the base metal at 77C	40
14	da/dN versus ΔK for the weld metal at 21C and -44C	41
15	da/dN versus ΔK for the weld metal at -14C and 81C	42
16	da/dN versus ΔK for the H.A.Z. at 21C and -48C	43
17	da/dN versus ΔK for the H.A.Z. at -13C and 86C	44
18	Load range versus crack length for a 21C base metal test	45
19	Irregular crack propagation in the -13C H.A.Z. test (X500)	46
20	Planar crack propagation for a 21C base metal test (X100)	47
21	Crack growth rate for $\Delta K = 63 \text{ ksi}\sqrt{\text{in}}$, as a function of temperature	48

LIST OF ILLUSTRATIONS (CONTINUED)

FIGURE		Page
22	Stress-intensity range for $da/dN = 8.9$ micro-inch/cycle, 50 as a function of temperature	
23	Results of one-hour static or cyclic strain-ageing on room temperature properties:	52
	(a) total elongation as a function of ageing temperature	
	(b) increases in yield strengths as a function of ageing temperature	

CHAPTER 1

INTRODUCTION

The modern trend in pipeline steels is towards high-strength, low alloy material that is grain-refined by addition of niobium or vanadium and by temperature-controlled rolling; this results in grain sizes that are orders of magnitude less than those of previously-used classical steels. At present, larger diameter pipe is favoured because of its great flowrate, thus necessitating ever-increasing yield strengths to compensate for the increased hoop stresses experienced in service. At present, steels of yield strengths exceeding 65 ksi are being placed into service.

One of the most common and insidious classes of mechanical failure is that of fatigue. A combination of a relatively small structural flaw and ordinary working stresses can lead to crack growth under fatigue conditions, resulting in catastrophic, abrupt failure. In a welded steel, there is ample opportunity for a fatigue crack to initiate and propagate, because of the internal weld defects and the impossibility of total non-destructive inspection. In areas of high local stress, a small but dangerous crack may be difficult to detect before it assumes critical proportions. In a technology that is very cost-conscious, it is not economical to design too carefully against crack initiation -- for example, circumspect reduction of the inclusion content of a steel may increase considerably the production costs and render a project completely uneconomical.

There is great concern about service failures of these steels, since a failure charged to a pipeline can very easily defeat the efforts of the

many who have tried prudently to design a structure economically. Due to the fact that failure is unannounced and that the pipeline crack may propagate unstably at speeds in excess of 1,000 feet per second, there have been proposals put forth suggesting the reduction of the presently-approved working pressures by as much as a factor of four (Ford, 1972); however, these proposals have not been well-received by the pipeline industry.

There has been very little study of fatigue crack propagation in welded steel, one reason being that a complete study would necessitate tests on the heat-affected zone (H.A.Z.), which is difficult to prepare for the standard test samples (Clark, 1969). A range of microstructures exists in and around the weld region, thus yielding a fatigue crack that does not propagate straight in the narrow and non-uniform H.A.Z. One method in use is that of producing a special "half-V" weld, resulting in a straight H.A.Z. (Gentilicore *et al.*, 1970); but due to the complex heating cycles experienced by the heat-affected metal of a multiple-pass weld, non-uniformity results. A second method that has been attempted is that of simulation of these heating cycles (Dolby, 1972; Bucci *et al.*, 1972). The author himself has conducted tests in which a furnace-heated sample was cooled in air, quenching oil, water, or between steel blocks; all of these investigations yielded structures that were of either much different hardnesses or of considerably different microstructures from the various regions of the H.A.Z. The approach followed in this present investigation was that of localized induction heating, followed by an air cool; this was found to be very satisfactory.

Fatigue crack propagation varies considerably with temperature (Andreassen, 1973); therefore, studies in this project were undertaken

over the wide range of temperatures experienced in practice by the material.

CHAPTER 2

EXPERIMENTAL PROCEDURE

2.1. Introduction

The purpose of this investigation was to study the effects of varying service temperature on the fatigue crack propagation rates in the base metal, weld metal, and H.A.Z. region of a fine-grained pipeline steel. The nominal test temperatures chosen were -45C, -10C, 21C, and 77C. In order to control the environment, the tests were conducted in prepurified, dried argon gas.

The data recorded from the tests included crack length as a function of fatigue cycles, and maximum and minimum bending moment.

A range of tensile tests was performed in order to assess the strain-ageing characteristics of the base material, since strain-ageing effects can be quite pronounced in very low carbon steel of small grain size.

2.2. Test Material

The test material was a section from a 42-inch O.D., 3/8" wall pipe that had been double-V submerged arc welded; it had been fabricated in conformation to American Petroleum Institute Standard 5LS -- X-65. The supply of this pipe by the Interprovincial Pipe and Steel Company is gratefully acknowledged. The base material was tested after press straightening and stress-relief annealing; the welded metal was tested in the as-received condition. The chemical composition and mechanical properties are listed in TABLE I; the mechanical properties as tested are given in TABLE II.

2.3. Microstructure

The microstructure of the as-received base material is shown in FIGURE 1; it consists of small patches of pearlite in a field of fine, equi-axed, ferrite grains. Due to rolling, there is a preferred grain orientation, as shown in FIGURE 2. The centre of the plate shows a concentration of carbon-rich regions (banding). The average grain size of a representative area is 0.315×10^{-3} inches (0.0080 mm), corresponding to an ASTM Micrograin size number of 11.0. FIGURE 3 shows the non-metallic inclusions, consisting of fine stringers of MnS, and blocky, massive silica. ASTM E-45 Method B was utilized for determination of inclusion representation as Type A, designation 1, indicating a very clean steel, virtually free of nonmetallic inclusions. The macrostructure of the weld is shown in FIGURE 4. The microstructure of the simulated H.A.Z., FIGURE 5, was virtually identical with that of the grain-coarsened H.A.Z. region of a weld done on the base plate, FIGURE 6; the hardnesses were also the same, as is given in TABLE II.

2.4. Heat Treatment

In an effort to reduce the residual stresses incurred by pipe rolling and the subsequent straightening, a stress-relief anneal of the base material was carried out at 1100 F (593C) for 40 minutes, followed by furnace cooling. Although this treatment raised the yield strength (as given in TABLE II) and produced a sharp yield point, other tensile properties were unchanged.

In order to reproduce the structure of the H.A.Z. and to simulate heat transfer conditions of the weld, the central region of a fatigue test specimen blank was heated to 2100F (1150C) in a single-turn coil of a radio-frequency induction furnace operating at approximately 10 kw

output power and 600 kc frequency. The specimen reached temperature within two minutes (as monitored by an infrared pyrometer) and was maintained in this state for $4\frac{1}{2}$ minutes. Cooling in air followed, the cooling curve being FIGURE 7, which shows the pearlite transformation beginning at approximately 700C and ending at about 600C. The simulated zone had a uniform microstructure over a range of approximately one inch of the sample length, ample to assure uniformity for testing; thus, the simulation was successful and satisfactory for the testing program.

2.5. Fatigue Test Specimen Preparation

Single-edge, notched specimens of dimensions 5.50" (14.0 cm) X 0.750" (1.90 cm) X 0.371" (0.942 cm) were machined from the plate in an orientation perpendicular to the rolling direction; this assured crack propagation along the rolling direction. The saw-cut surfaces were milled flat to guarantee that all faces were 90 degrees to each other. A starter notch was introduced as a stress concentrator by the drilling of a 0.025" (0.64 mm) hole a distance of $\frac{3}{32}$ " (2.4 mm) in from the edge at the centre of the specimen length. A fine saw was utilized for cutting outwards from this hole to the specimen edge, leaving a keyhole notch. The sides of the specimen were polished to Number 600 grit abrasive in order to produce a mirrored surface, enhancing observation of the crack during testing. For testing the weld metal and the H.A.Z. samples, the notch was placed in the centre of the welded zone and H.A.Z., respectively. In no instance did the crack deviate from a transverse plane.

2.6. Static and Dynamic Tensile Tests

The purposes of this section of the investigation were to assess the tensile properties of the grade 65 steel and to study strain-ageing

effects. Round tensile specimens were produced by cutting and machining from the plate such that the specimen axis was parallel to the rolling direction. The samples, of gauge length 1.5" (3.8 cm) and reduced section 0.2" (0.5 cm), contained threaded ends so that they could be secured in mating grips on an Instron tensile testing machine.

The tensile properties of the base material were tested in "as is" condition and after strain-ageing; other samples were stress-relieved and subjected to the same types of test.

The strain-ageing tests were carried out with similar specimens, which were strained initially to 4% permanent strain. Then, a sample was brought to ageing temperature (The ageing temperatures chosen were 0F (-18C), 75F (24C), 212F (100C), and 400F (204C).) under either tensile load or fatigue cycling for one hour at pulsating stress equivalent to the prior flow stress. After returning the sample to room temperature, it was strained a further 1%. Following further ageing under the same conditions, it was fractured. Crosshead speed was 0.10 inches (2.54 mm) per minute and the fatigue cycle frequency was 2.5 per minute. This double strain-ageing test provided more information than could have been obtained from a more conventional procedure.

2.7. Calculation of Stress-intensity Factor

The stress-intensity factor, K , used in the fatigue analysis is that derived by Kies *et al.* (1965):

$$K = \frac{AM}{tW^{3/2}} \sqrt{1/\alpha^3 - \alpha^3}$$

where A is 4.12 for cantilever bending, M is the bending moment, t is the specimen thickness, W is the width, and $\alpha = 1 - a/W$, where a is the

length of crack plus notch. The equation is valid for the plane strain fracture mode, in which the thickness of test specimen should be at least fifteen times the extent of the plastic zone ahead of the crack. All plastic yielding is constrained to this zone due to the great amount of surrounding material that resists lateral contraction of the specimen along the crack front. Previous work (such as that by Andreassen, 1973) has shown that the plastic zone in steel is small, especially in tensile fatigue. Indirect evidence of plane strain conditions is given by the linearity of the curve of load range versus the crack length, FIGURE 18. Measurements were obtained after the crack was beyond the stress field of the starter notch. As the crack approaches $a/W = 0.5$, it senses the stress field of the far edge of the specimen and the plastic constraint decreases. Thus, no testing was done beyond this region.

2.8. Testing Machine and Fatigue Testing Procedure

Fatigue testing was conducted in a 640 cpm, constant deflection fatigue bending machine, of which FIGURE 8 is a schematic illustration and FIGURE 9 is a photograph, showing the specimen orientation in the machine. The specimen was mounted vertically, with a moment arm attached to the upper part. A variable eccentric was employed for moving a connecting rod that activated the moment arm. Two parallel eccentrics could be adjusted for desired minimum load and load amplitude. Four B.L.H. SR - 4 strain gauges were mounted on the connecting rod, their output being monitored on a Tektronix 561B cathode ray oscilloscope with a 3C66 carrier amplifier. For measurement of the load amplitudes, settings of 20 microstrain/div and full gain of the oscilloscope were used.

Testing was carried out in a lucite chamber containing a glass

observation window and a passageway for a thermocouple. A flexible seal between the chamber and the moment arm was provided by a thin, rubber cylinder. Throughout all tests, the sample chamber was flushed with argon gas that passed through a Matheson Model 450 dryer and a cylinder of anhydrous CaSO_4 dessicant to remove additional moisture. A back pressure was provided by passing the exit gas through a tube submerged in oil. The impurity composition of the gas is given below:

IMPURITY	CONTENT (parts per million)
oxygen	5
water	5
hydrogen	1
hydrocarbons	1
carbon dioxide	1
nitrogen	0

In order to control the test specimen temperature, the bottom part of the grips was seated in a forked copper rod that extended downwards. The rod could be submerged in a Dewar flask containing liquid nitrogen, dry ice in acetone, ice water, or heated paraffin oil. Temperature was monitored by a copper-constantan thermocouple attached to the specimen near the crack plane.

A small ruler with $1/64$ " (0.400 mm) divisions was placed in the specimen chamber to allow measurement of crack lengths with a 20-power travelling telescope. Crack lengths could be measured to a precision of 0.1 scale division (0.00156" or 0.0400 mm) and these measurements were secured every one-half minute (or about every 300 fatigue cycles).

CHAPTER 3

EXPERIMENTAL RESULTS

3.1. Crack Length versus Number of Fatigue Cycles

In FIGURE 10 is shown a plot of crack length, a , versus the number of fatigue cycles, N , for the welded specimens; those for the base plate and the H.A.Z. samples were identical in nature. Three regions can be seen on the curves: an initial section depicting low crack growth rate, a region of increasing crack growth rate, and a final region during which the load was decreasing so that the crack growth rate was not increasing. The initial section was not used in the analysis, due to the influence of the stress field around the machined notch. From these curves, the crack growth rate, da/dN , was obtained by calculating the instantaneous slope of the curve at various values of crack length. In constant deflection amplitude tests, both the load and the stress-intensity vary as the crack advances; thus, for every value of crack length, there is a corresponding stress-intensity.

3.2. Crack Growth Rate versus ΔK

Plane strain fatigue crack propagation is conventionally represented within a certain range of stress-intensity, $\Delta K = (K_{\text{maximum}} - K_{\text{minimum}})$ by the expression

$$da/dN = C (\Delta K)^m$$

where C and m are material constants. Commonly, $\log(da/dN)$ is plotted against $\log(\Delta K)$. This power-law region of fatigue crack growth is bounded on both ends by inflection points, the upper and lower regions

signifying the zones of unstable propagation and non-propagating cracks, respectively. The lower bound (threshold) stress-intensity, K_{th} , has been accounted for by Donahue *et al.* (1972):

$$da/dN = C (K - K_{th})^2$$

Shown in FIGURES 11, 12, and 13 are plots of only the central portion of da/dN versus ΔK for the base metal tests at 21C, -48C and -7C, and 77C, respectively. There exists a wide variation between room temperature tests, as there is between the -48C tests; this is because da/dN varies rapidly with incremental changes in temperature in these temperature ranges (See FIGURE 21.). FIGURES 14 and 15 are plots for the steel weldment tests at 21C and -44C, -14C and 81C, respectively; these curves all show a definite trend and exhibit little scatter. FIGURES 16 and 17 are plots for the H.A.Z. tests at 21C and -48C, -13C and 86C, respectively. Greater scatter exists in these plots, but the power-law behaviour is evident.

The scatter in any base metal test or weld test is seen to be very small, usually approaching data correlations of greater than 99%. Experimental scatter was reduced by plotting the alternating load versus the crack length and selecting the least-squares-best-fit straight line through the data, as shown in FIGURE 18. Assuming random scatter due to the inability to record crack lengths and load amplitudes without error, this approach is justified, since from mechanical principles, the load decreases linearly in plane strain as the crack extends. It can be seen that the scatter is greater for the H.A.Z. tests; this is due to the fact that there was branching of the crack as it propagated, as shown in FIGURE 19. The other material exhibited planar propagation, as is shown

for a base metal crack, FIGURE 20. For irregular propagation, such as the branching of the crack in the H.A.Z., the use of linear-elastic fracture mechanics is questionable; nevertheless, it has been applied in order to compare with the other data.

CHAPTER 4

ANALYSIS AND DISCUSSION

In the past, fatigue studies of welded structures have been devoted to developing mainly "S-N" curves (Munse, 1964; Gurney, 1968a). Notched H.A.Z. studies of mild and low alloy steel have shown fatigue strengths equal to those of the weld metal (Kenyon *et al.*, 1966).

The limited amount of previous work on fatigue crack propagation in weldments has been done on thick, centre-notched plates loaded axially (Gurney, 1968a, 1968b; Maddox, 1970). Recently, fracture mechanics has come into wide use in the study of fatigue of welded structures (Maddox, 1969; Wessel, 1969; Harrison, 1969; Fisher, 1970; and Tall, 1970). Nibbering and Lalleman (1970) propagated cracks through the coarse regions of the H.A.Z. "Brittle steps" were found, corresponding to heterogeneity of structure and to the cyclic loading. Some heat-affected zones were simulated by Bucci *et al.* (1972) by austenitizing a sample for one hour at 2300F, followed by a water quench and then a 24-hour stress relief at 950F. Unfortunately, these authors do not prove in any manner that the resulting structure compares to an actual H.A.Z. Those who did tests with real H.A.Z. samples did not indicate how they prepared a H.A.Z. sufficiently straight and wide for a fatigue crack to pass without deviation. Of those who did fracture mechanics studies of fatigue crack propagation in weld, H.A.Z., and base metal, data were scanty and no statement was made as to the influence of temperature. As a result, there is little comparison that can be made with the results reported.

Values of da/dN for a given ΔK are plotted as a function of testing temperature for all tests, FIGURE 21. It can be seen that for a given ΔK , a maximum crack propagation rate occurs in the temperature region of -7°C . In the temperature interval of -7°C to 32°C , the crack propagation rate decreases drastically -- especially for the base metal -- until about 32°C , where it reaches a minimum. Values of ΔK for a given da/dN , shown in FIGURE 22, exhibit an inverse trend to the curves of FIGURE 21.

The increase of ΔK for a given da/dN in the temperature interval of -7°C to 32°C may be explained by dynamic strain-ageing. However, a decrease is observed at a relatively low temperature, 32°C . Such a peak in values of the fatigue strength due to strain-ageing has been previously observed in the blue brittle temperature range of 200°C to 300°C (Forrest, 1957). The decrease beyond the peak temperature is explained by over-ageing. Although strain-ageing has been reported down to -60°C (Mintz and Wilson, 1965), no drop-off in the temperature range -7 to 32°C observed in this investigation has been reported in the literature. No evidence of a specific mechanism is available, but it is suggested that an ageing reaction of the Cottrell dislocation locking type, by nitrogen, may be the cause of the observed behaviour.

For further discussion of the trend shown by FIGURES 21 and 22, the influence of the yield strength on crack propagation rate will be explained on the basis of equations proposed for the mechanism of crack propagation. This is followed by a discussion of ageing reactions under fatigue conditions.

The relevant variables for crack propagation in a body are the range of stress ($\Delta\sigma$), crack length (a), yield stress (σ_0), yield strain (ϵ_0),

characteristic fracture strain (ϵ_f), strain-hardening exponent (n), and crack growth rate (da/dN). Since the stress distribution at the leading edge of the plastic zone is uniquely defined by the stress-intensity factor (K) and the stress at a finite distance from the crack tip is proportional to K , then the crack growth rate in fatigue is related to K . This has been displayed by Liu (1961) as:

$$da/dN = f(\Delta K/\sigma_0, \epsilon_0, \epsilon_f, n)$$

Paris (1964) found experimentally that da/dN varies as ΔK^4 ; other researchers (Head, 1956; Weibull, 1963; and others) have verified this power-law relationship. Although Paris' equation fits most experimental data, no commonly accepted model has been postulated to derive it. It can be seen from the preceding equation that the effect of yield strength is quite pronounced; if strain-ageing were to increase the value of σ_0 , then the value of da/dN would decrease for any given ΔK . Bilby and Heald (1968) developed the relationship:

$$da/dN = \frac{5\pi^3 K^2}{192G\gamma\sigma_u^2}$$

where γ is the surface energy of the material, G is the crack extension force, and σ_u is the ultimate tensile strength. A similar relationship was put forward by Lardner (1968):

$$da/dN = \frac{(1 - \nu) K}{4G\sigma_u} \left(1 + \frac{\pi^3 \sigma_u^2}{96\sigma_u^2}\right)$$

Rice (1967) derived the relationship:

$$da/dN = \frac{5 \pi^3 (1 - \nu^2) K^2}{96 U^* \sigma_0^2}$$

where U^* is the critical hysteresis energy required per unit area of new surface. Tompkins (1968) developed the following equation for conditions of high amplitude, plastic stress cycling:

$$da/dN = \frac{\pi}{32} \frac{\epsilon_f}{\sigma_f^{1/n} \sigma_0'} \Delta \sigma \left(\frac{2n+1}{n} \right)$$

where σ_f is the true fracture strength and σ_0' is the cyclic flow stress. Relationships have been developed to account for the influence of the strain to fracture (McClintock, 1963; McEvily and Johnson, 1965; and Rice, 1965); but since the strain to fracture under static conditions cannot be compared with that which results from fatigue conditions (due to such effects as the difference in strain history of the plastic zone of the crack), these relationships are beyond consideration in the present analysis. The above equations indicate that for a given ΔK , there is a decrease in da/dN as the yield strength increases.

To investigate the effect of dynamic strain-ageing on the yield strength of the present steel, several exploratory tests were conducted. The procedure for the strain-ageing tests was outlined in SECTION 2.6. It was found that no sharp upper yield point occurred after static ageing for one hour at temperatures ranging from -18C to 204C, but a distinct yield point was observed after fatigue loading. The increase in both the upper and lower yield stresses after both static and dynamic ageing is shown as a function of ageing temperature, in FIGURE 23; the total

elongation at fracture as a function of ageing temperature is also plotted. These tests, although of an exploratory nature, exhibit a trend which lends support to an explanation of the variation of da/dN in FIGURE 21, on the basis of a strain-ageing reaction. The increase in tensile yield strength after ageing (FIGURE 23b) indicates that the magnitude of the increase at any ageing temperature is much greater in the fatigue ageing than in the static ageing. The total elongation to fracture decreased slightly with ageing temperature for the static tests, but the drop-off was significant for the dynamic tests (FIGURE 23a). Applying the above equations to FIGURE 23b, the increase in yield strength after the second ageing rises with ageing temperature from -170°C to 210°C , resulting in a lower crack propagation rate for a given stress-intensity, due to strain-ageing. As ageing temperature rises further, the increase in yield strength drops, resulting in a greater crack propagation rate for a given stress-intensity, due to overageing.

The increase in tensile properties due to dynamic strain-ageing has been noted by many investigators (for example, Levy and Sinclair, 1955; Forrest, 1957; Hundy and Boxall, 1957; Levy, 1957; Thompson and Wadsworth, 1958; Adair and Lipsitt, 1966; Barnby, 1966; and Baird, 1963, 1971). It can be seen that the increase in yield strength for the second straining is less for the ageing above room temperature; this can be explained as overageing, which leads to a decrease in the fatigue properties of the material. This effect was observed in the same region as the increase in da/dN for constant ΔK , in FIGURE 21. Overageing was observed also in low-carbon steel at 970°C by Klesnil and Rys (1961). By measuring hardness, they determined that precipitation of carbide from a supersaturated, solid solution of alpha iron in steel was greater as

temperature was lowered from 128C to 23C, even though the reaction rate decreased; however, cold plastic deformation (20% strain) was sufficient to increase both the hardness and the rate of precipitation by a very considerable amount. The effect increased with load amplitude, probably due to an increase in temperature in the slip bands, because of moving dislocations. Overageing was found to occur when the static heating was carried out for too long. This was observed also in this project, as shown by the reduced increase in yield strength for the second straining after ageing. The overageing manifests itself in the decrease in fatigue strength observed (as given by the decrease in ΔK for a given da/dN , FIGURE 22) for the fatigue tests conducted at high temperature. Doremus (1960), measuring carbon precipitation from alpha iron with low carbon content, found evidence of the occurrence of a different mode of nucleation below 60C. Riccardella and Mager (1972) observed the same behaviour as is exhibited in the curves of FIGURES 21 and 22, but at much higher temperatures; this was undoubtedly due to the strong strain-ageing effect of carbon at these temperatures.

Mintz and Wilson (1965) found an ageing reaction occurring at temperatures as low as -60C. Fatigue ageing was found to be at least an order of magnitude more rapid. These authors suggested that this strain-ageing was due to carbon derived from the re-solution of fine carbide particles in regions of active slip. Local heating in these areas could provide the activation energy required for the ageing reactions. Oates and Wilson (1964) detected a temperature rise on the order of 60C degrees in the vicinity of the crack tip; however, the thermocouple employed for these measurements could not probe as minute a volume as the plastic zone. On the basis of hysteresis loop measurements, Andreasen (1973)

calculated a temperature rise in excess of 300C degrees; similar results have been obtained by Freudenthal and Weiner (1956). Modlen and Smith (1960) recorded a temperature rise of 200C degrees in a steel sample undergoing axial fatigue.

From FIGURE 21, the increase in da/dN for a given ΔK as test temperature rises from -48C to -7C, is therefore explained as being due to the decrease in yield strength. The dropoff (especially for the base metal) is likely due to strain-ageing, which increases the yield strength of the material. Above about 20C, the decrease in yield strength, which causes an increase in the crack propagation rate for a given ΔK , may be caused by overageing.

Strain-ageing can be caused by either or both carbon and nitrogen diffusion to dislocations. It is well known that carbon is responsible for strain-ageing at much higher temperatures than those commonly employed in this investigation; thus, nitrogen-induced ageing is the more likely mechanism. In the temperature range studied, the equilibrium solubility of nitrogen in ferrite is on the order of 100 times that of carbon in ferrite; furthermore, the diffusion of nitrogen in ferrite is about four times faster than that of carbon (Fast, 1965). Thus, nitrogen-induced strain-ageing would be much more pronounced. Niobium is a strong former of carbides and nitrides; in fact, 0.36% Nb is sufficient to eliminate strain-ageing effects and the initial yield (Hall, 1970). However, the niobium content of the present steel (0.06%) is much too small to tie up the available nitrogen. Chemical analysis of the steel tested revealed a nitrogen content of 0.013 percent, which is substantial. Thus, nitrogen strain-ageing could be a possible explanation for the observed results. In fact, it is possible that this is the mechanism

influencing the results of other investigators who witnessed strain-ageing at temperatures much below those at which carbon strain-ageing is normally observed.

CHAPTER 5

SUMMARY AND CONCLUSIONS

The main conclusions of this study of cyclic bending fatigue crack propagation for the temperature range of -48C to 86C, in API 5LS -- X-65 base metal, heat-affected zone, and Linde No. 36 weld metal, are as follows:

1. Since decreased da/dN for a given ΔK at any temperature is indicative of increased fatigue resistance, the weld metal is the most resistant to fatigue crack propagation, followed by the heat-affected zone and the base metal.
2. For a given stress-intensity range, fatigue crack propagation rate in the base metal increases considerably from -48C to -7C, decreases from -7C to 32C, then increases with temperature to 77C. The fatigue crack propagation rate in the weld and the heat-affected zone does not change significantly with temperature.
3. The increase in da/dN for a given ΔK in the region of -48C to -7C is believed to be due to the decrease in yield stress. From -7C to 32C, dynamic strain-ageing effects an increase in flow stress, which decreases da/dN . From 32C to 77C, overageing is believed to occur, decreasing the flow stress and thus increasing the fatigue crack propagation rate.
4. Further study is essential in other regions of crack propagation rates and other temperature regions for this material. Also, studies of fatigue crack propagation as a function of temperature are conspicuously lacking; therefore, more attention must be given to them, since strain-ageing may have a great effect on crack

propagation mechanism. The effect of nitrogen in fatigue strain-ageing must be investigated further. Most investigators assert (without proof) that carbon is the species active in the process, but they do not give due consideration to the rôle that nitrogen may play in the ageing reaction observed.

TABLES

TABLE I

CHEMICAL COMPOSITION OF TEST MATERIAL
(as provided by IPSCO, unless otherwise indicated)

Base Metal:

ELEMENT	WEIGHT PERCENT
carbon	0.06 (0.08*)
manganese	1.50
niobium	0.06
phosphorus	0.024
sulfur	0.015
nitrogen	0.013*

Weld Metal (Linde No. 36):

carbon	0.14 (0.05*)
manganese	2.0
phosphorus	0.011
sulfur	0.024
silicon	0.3
nitrogen	0.014*

(* Analysis performed by Chicago Spectro Service Laboratory, Inc.,
Chicago, USA.)

MATERIAL PROPERTIES AT ROOM TEMPERATURE
(as provided by IPSCO)

PROPERTY	ROOM TEMPERATURE VALUE
yield strength	77.5 ksi (535 MN/m ²)
tensile strength	93.9 ksi (660 MN/m ²)
total elongation	0.34 in/in

TABLE II

TESTED TENSILE PROPERTIES OF BASE METAL

PROPERTY	ROOM TEMPERATURE VALUE
As received:	
lower yield strength	74.0 ksi (520 MN/m ²)
tensile strength	92.5 ksi (650 MN/m ²)
total elongation	0.265 in/in
Stress-relieved:	
upper yield strength	85.5 ksi (601 MN/m ²)
tensile strength	94.4 ksi (664 MN/m ²)
elongation	0.267 in/in
Vickers hardness of the grain-coarsened region of the H.A.Z.: 223	
Vickers hardness of the simulated H.A.Z.: 218	

FIGURES



FIGURE 1: Microstructure of the as-received base material (X500)



FIGURE 2: Preferred grain orientation and banding in base metal
(X100)



FIGURE 3: Nonmetallic inclusions of the base metal (X100)

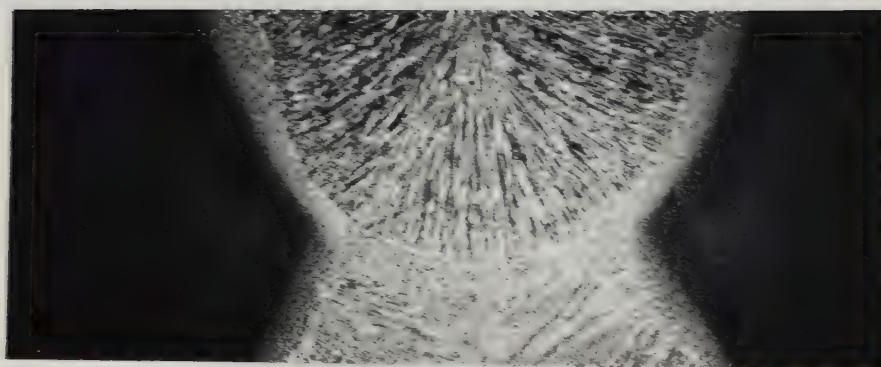


FIGURE 4: Macrostructure of the weld (X5)

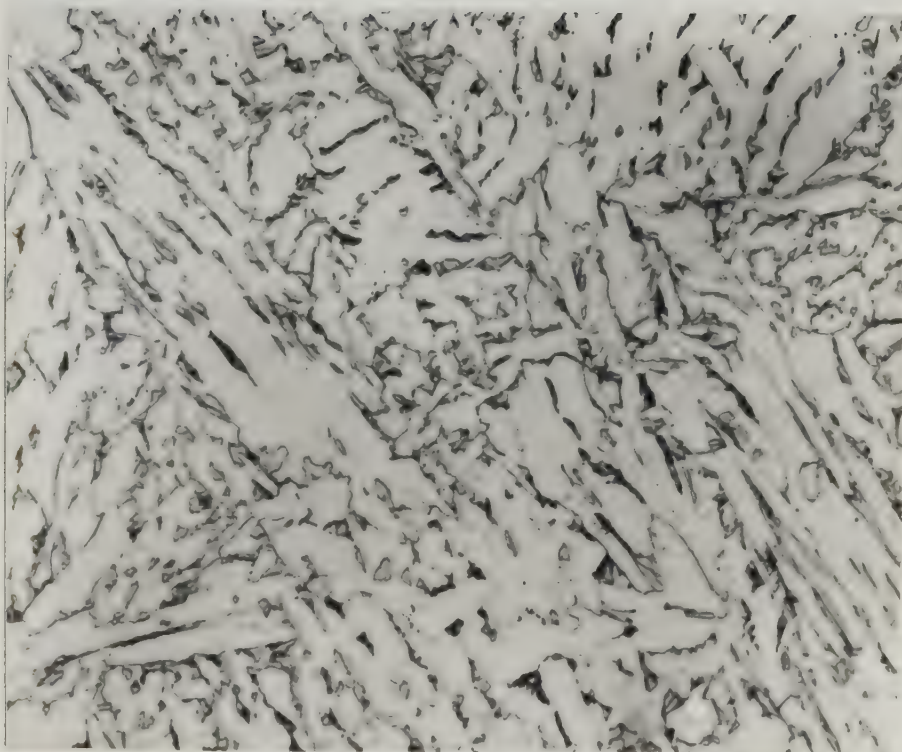


FIGURE 5: Microstructure of the simulated heat-affected zone (X500)

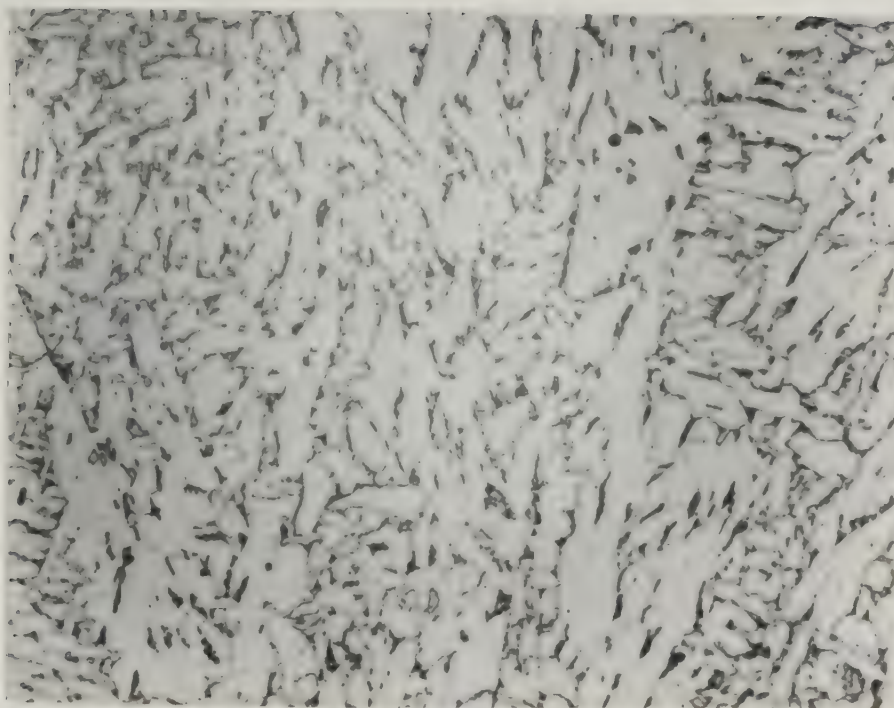
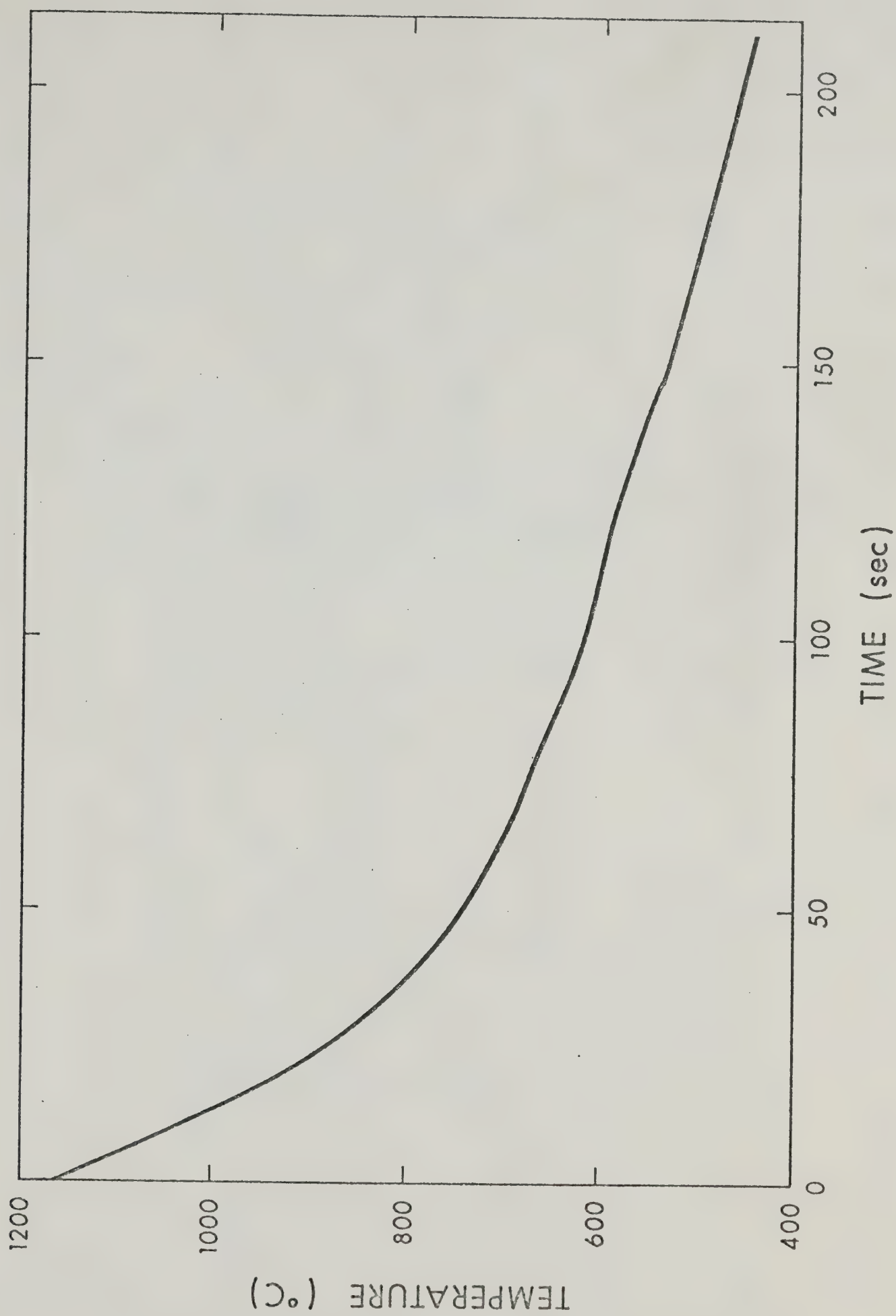


FIGURE 6: Microstructure of the grain-coarsened H.A.Z. of the weld (X500)

FIGURE 7: Cooling curve of the induction-heated, simulated H.A.Z.



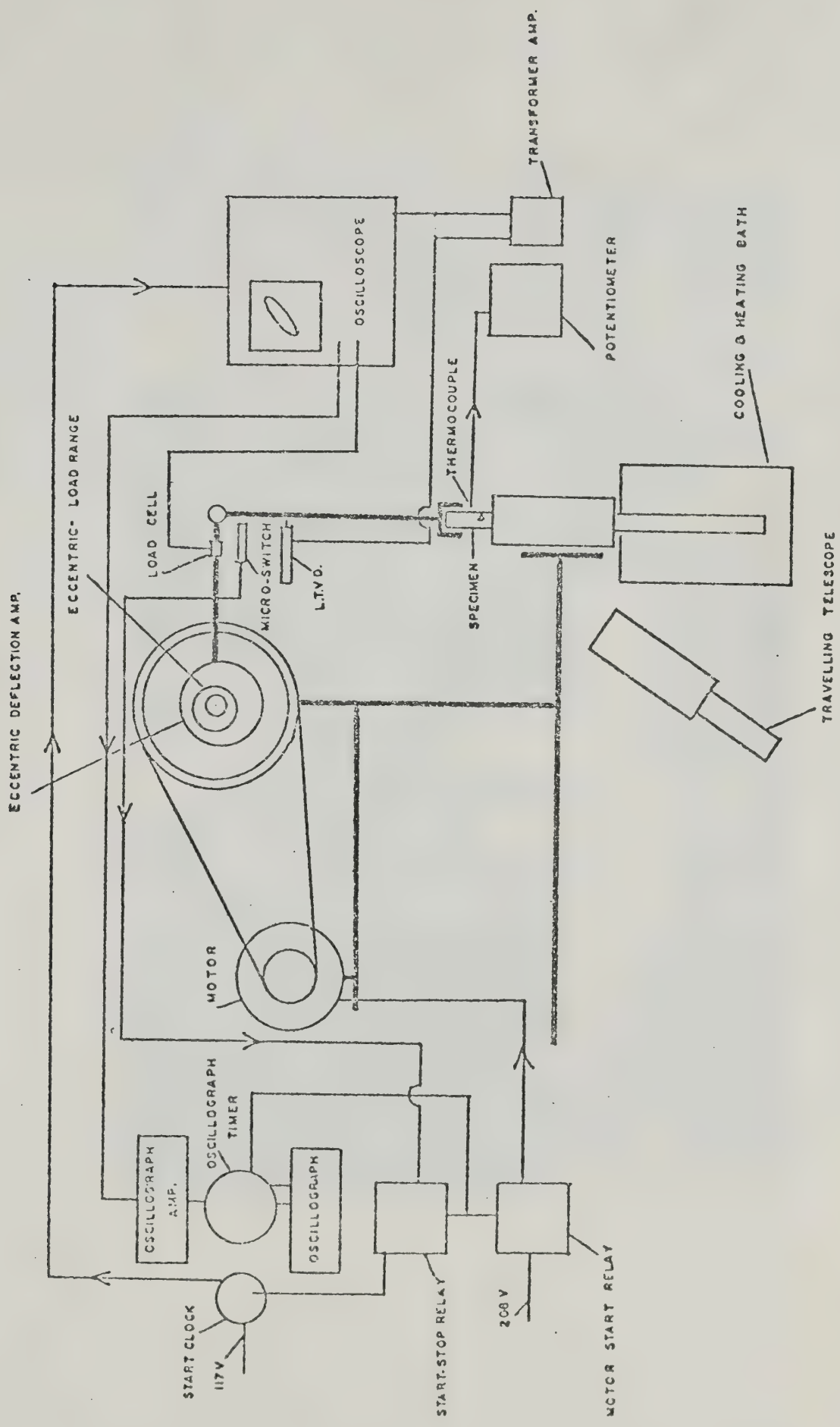


FIGURE 8: Schematic illustration of the fatigue testing machine (after Andreassen, 1973)



FIGURE 9: Fatigue testing machine, showing specimen orientation

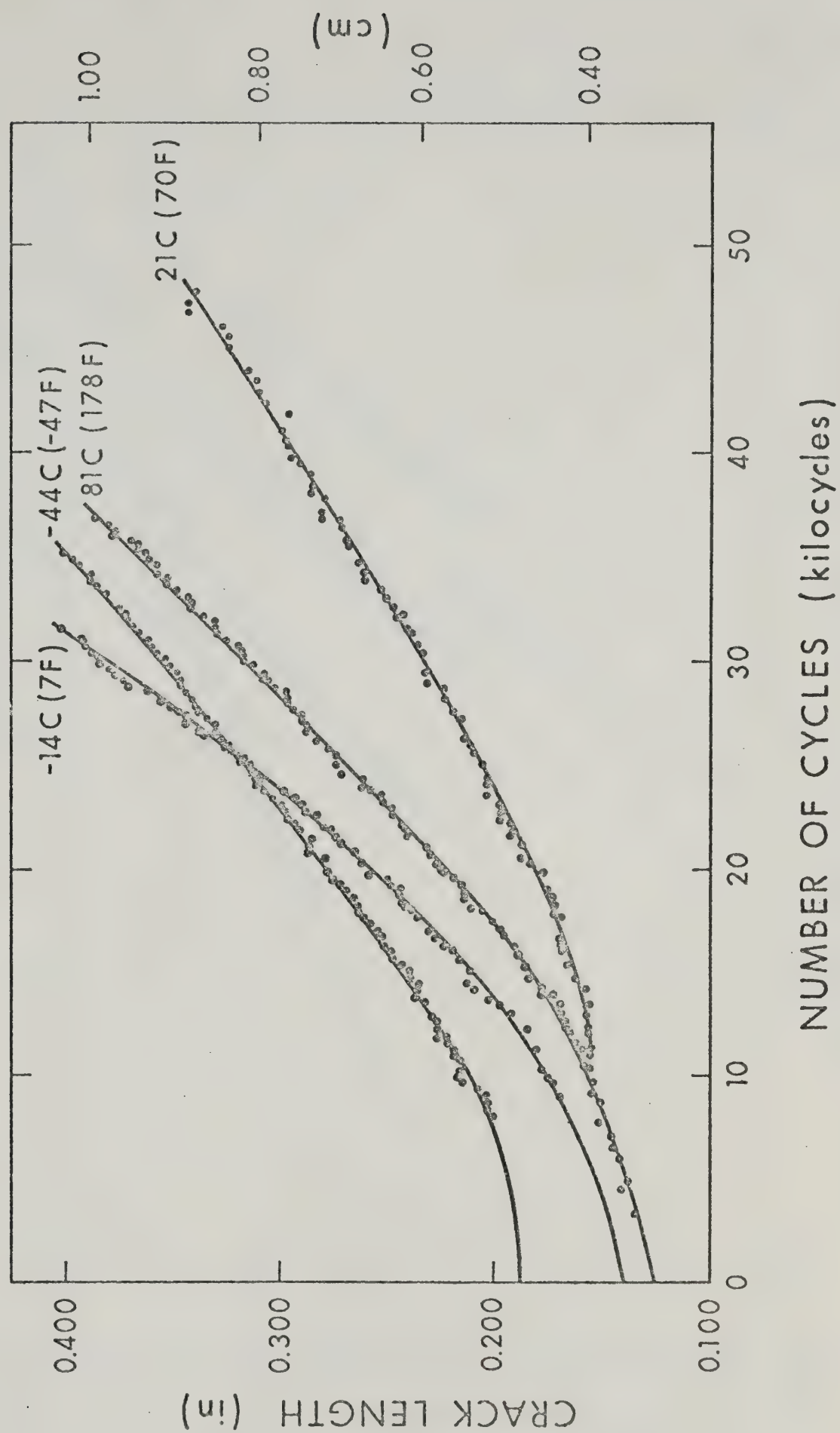


FIGURE 10: Crack length versus fatigue cycles, for welded samples

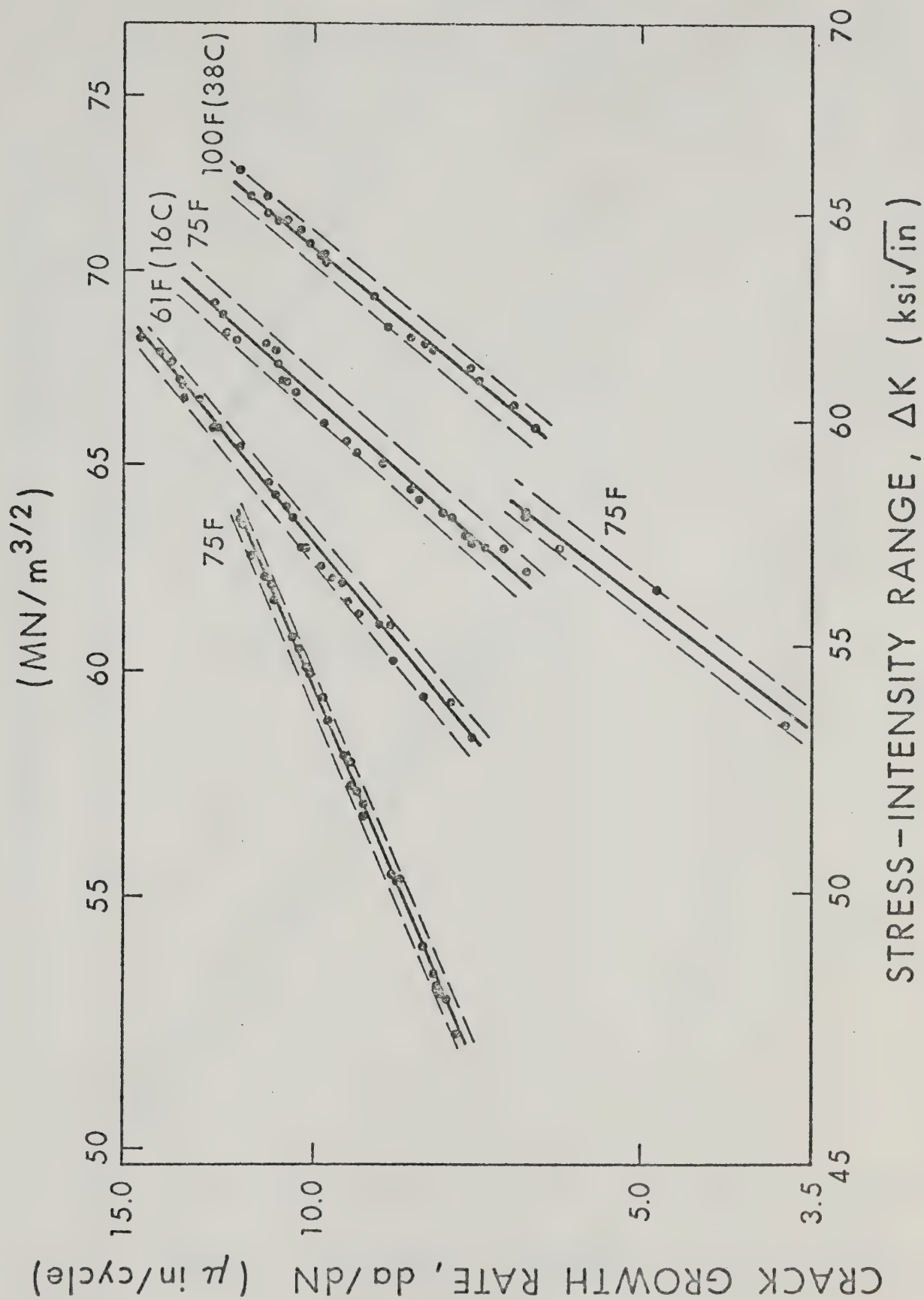


FIGURE 11: Crack propagation rate as a function of stress-intensity range for the base metal at 21C

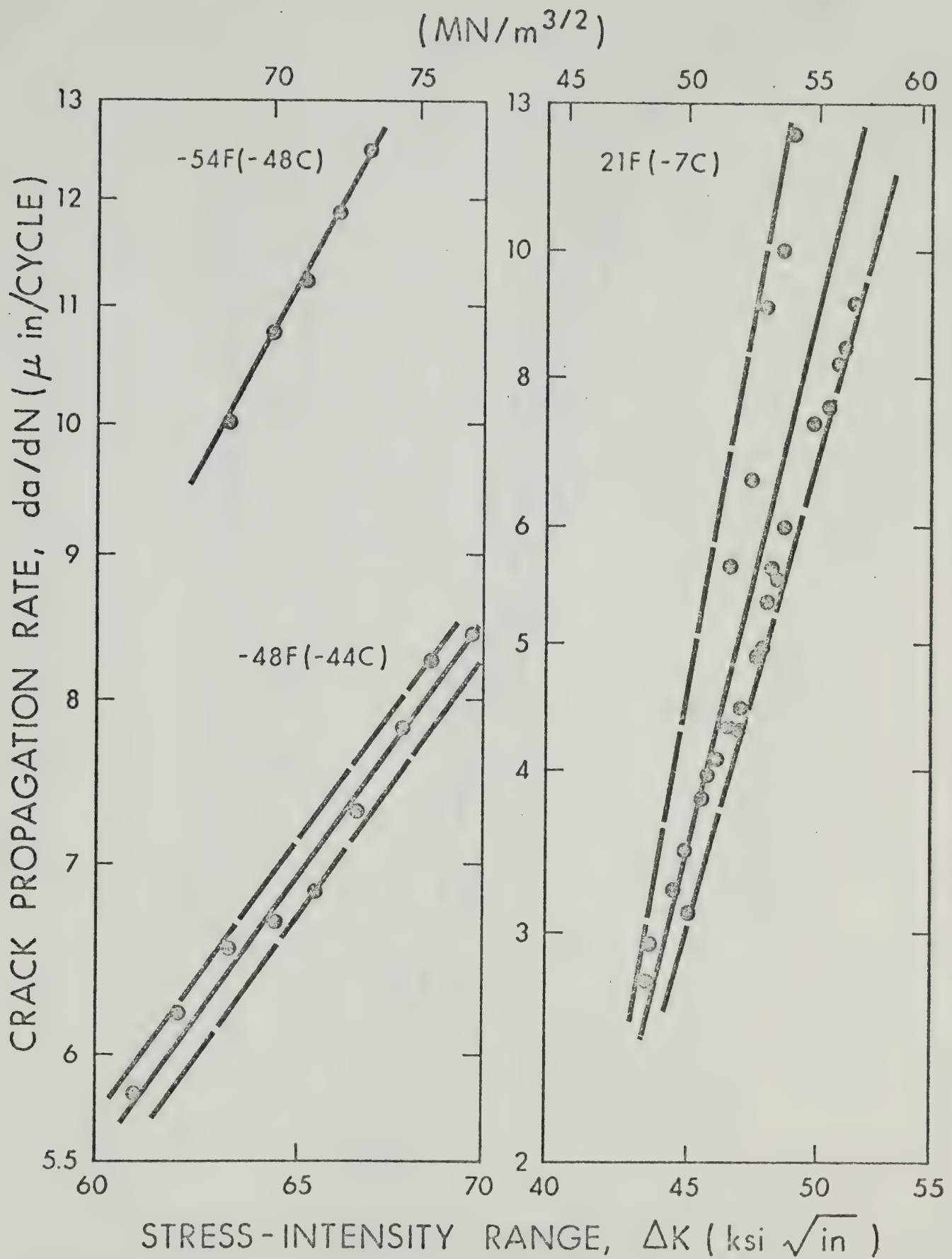


FIGURE 12: Crack propagation rate as a function of stress-intensity range for the base metal at -48C and -7C

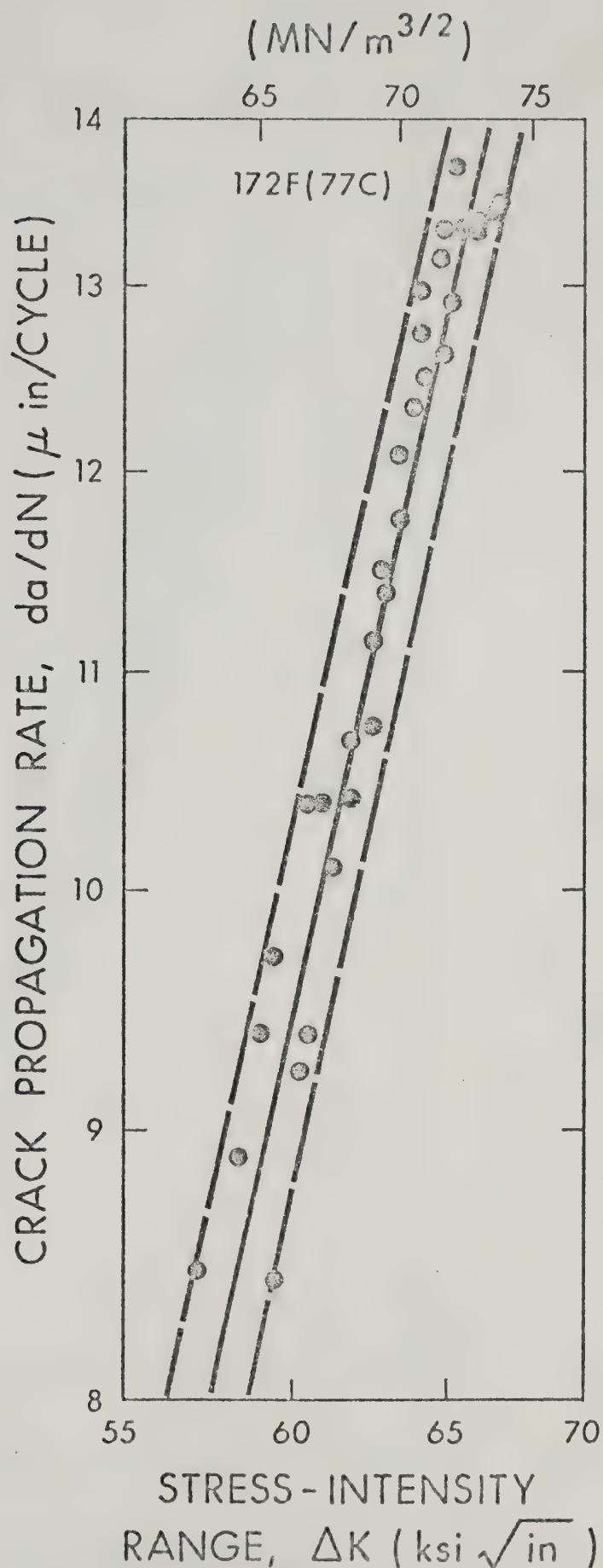


FIGURE 13: Crack propagation rate as a function of stress-intensity range for the base metal at 77C

(MN/m^{3/2})

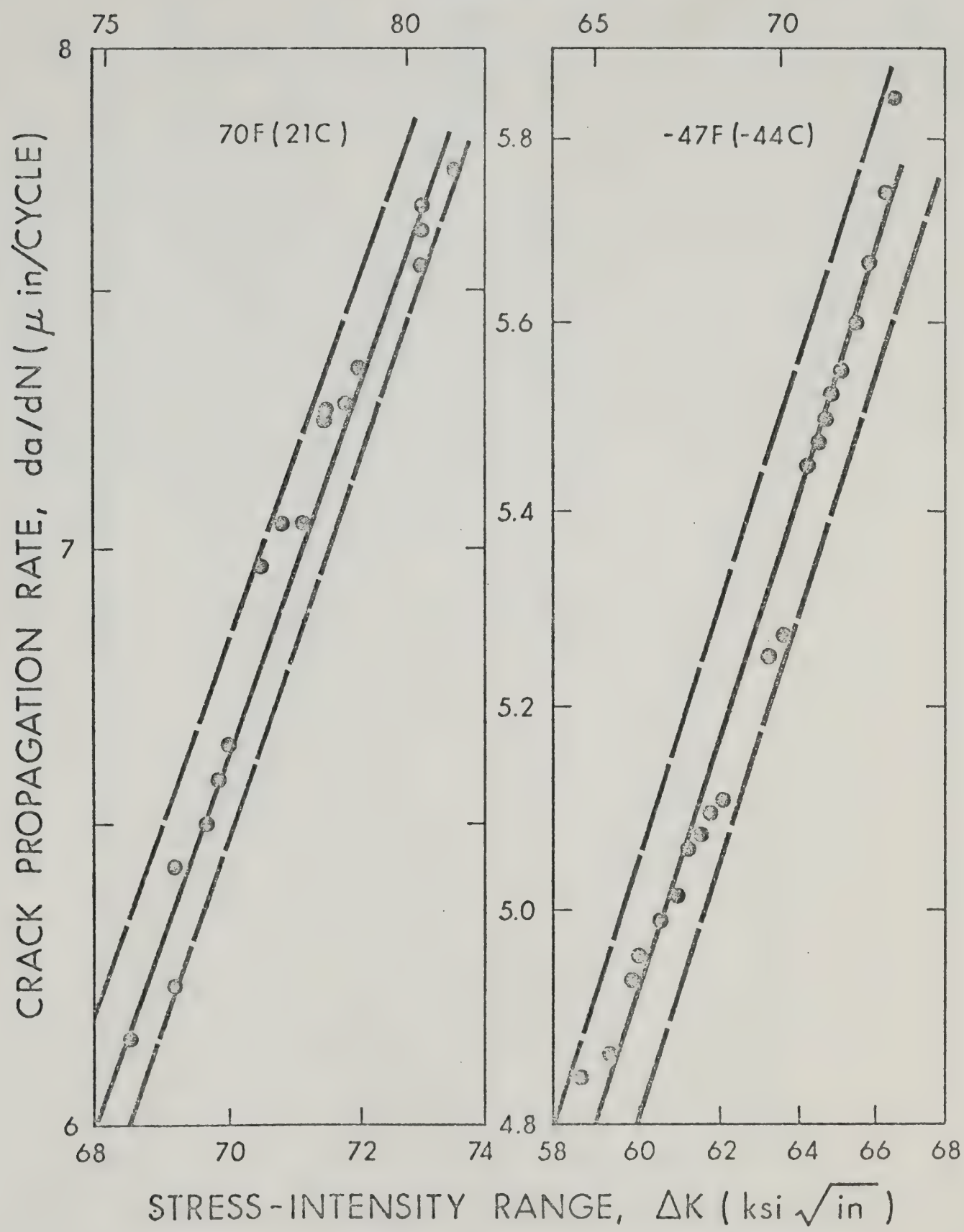


FIGURE 14: Crack propagation rate as a function of stress-intensity range for the weld metal at 21C and -44C

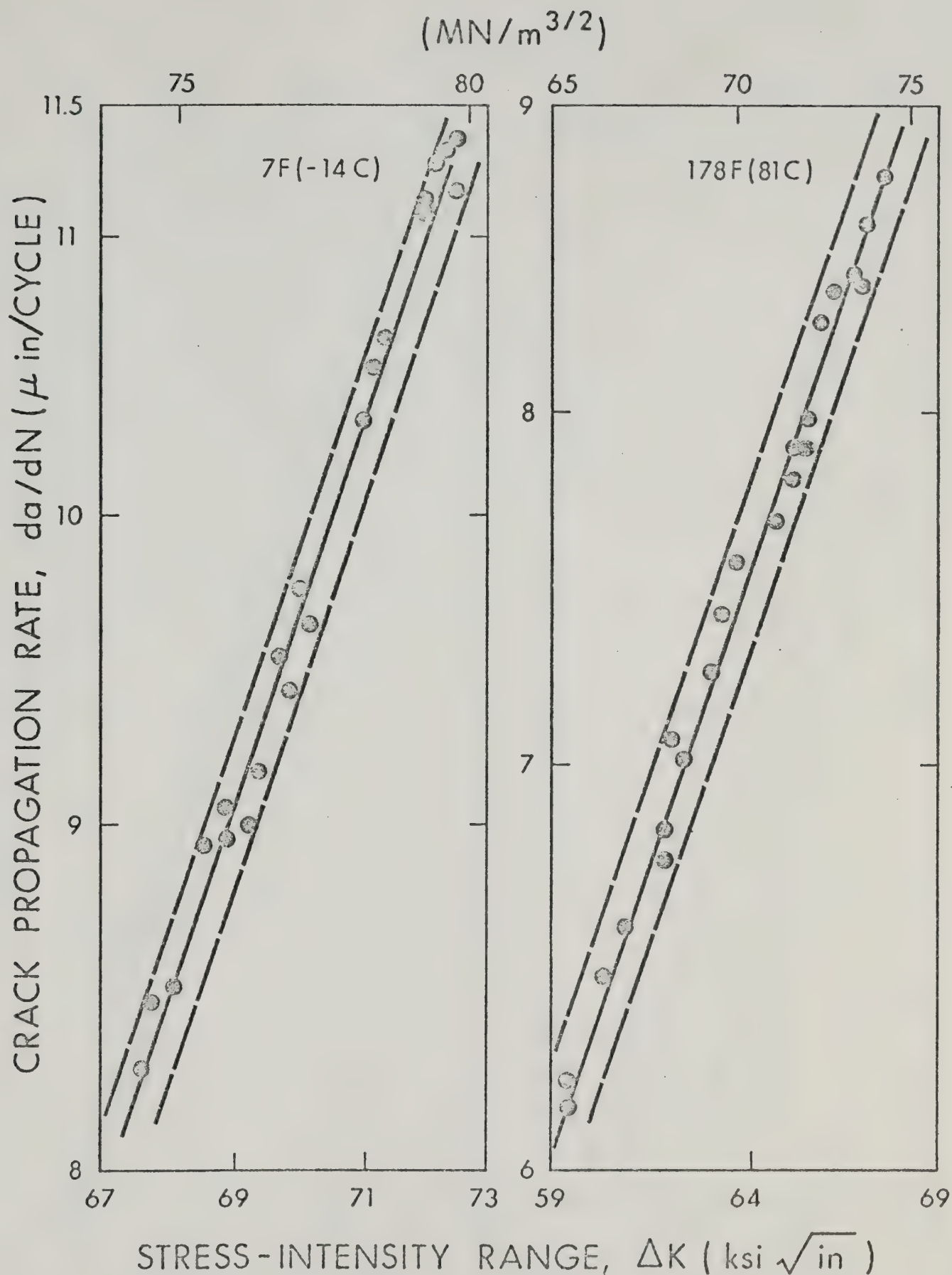


FIGURE 15: Crack propagation rate as a function of stress-intensity range for the weld metal at -14C and 81C

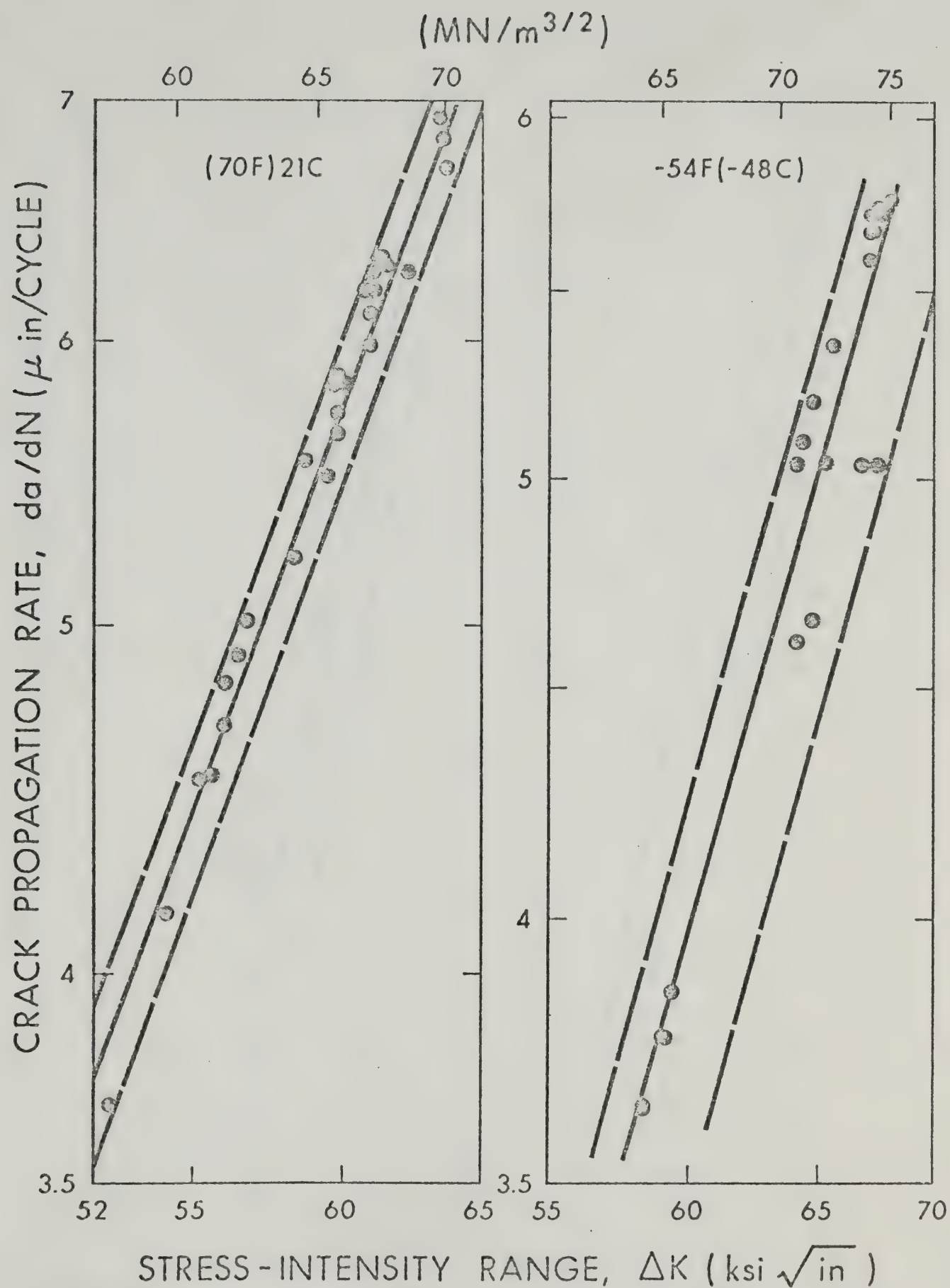


FIGURE 16: Crack propagation rate as a function of stress-intensity range for the H.A.Z. at 21C and -48C

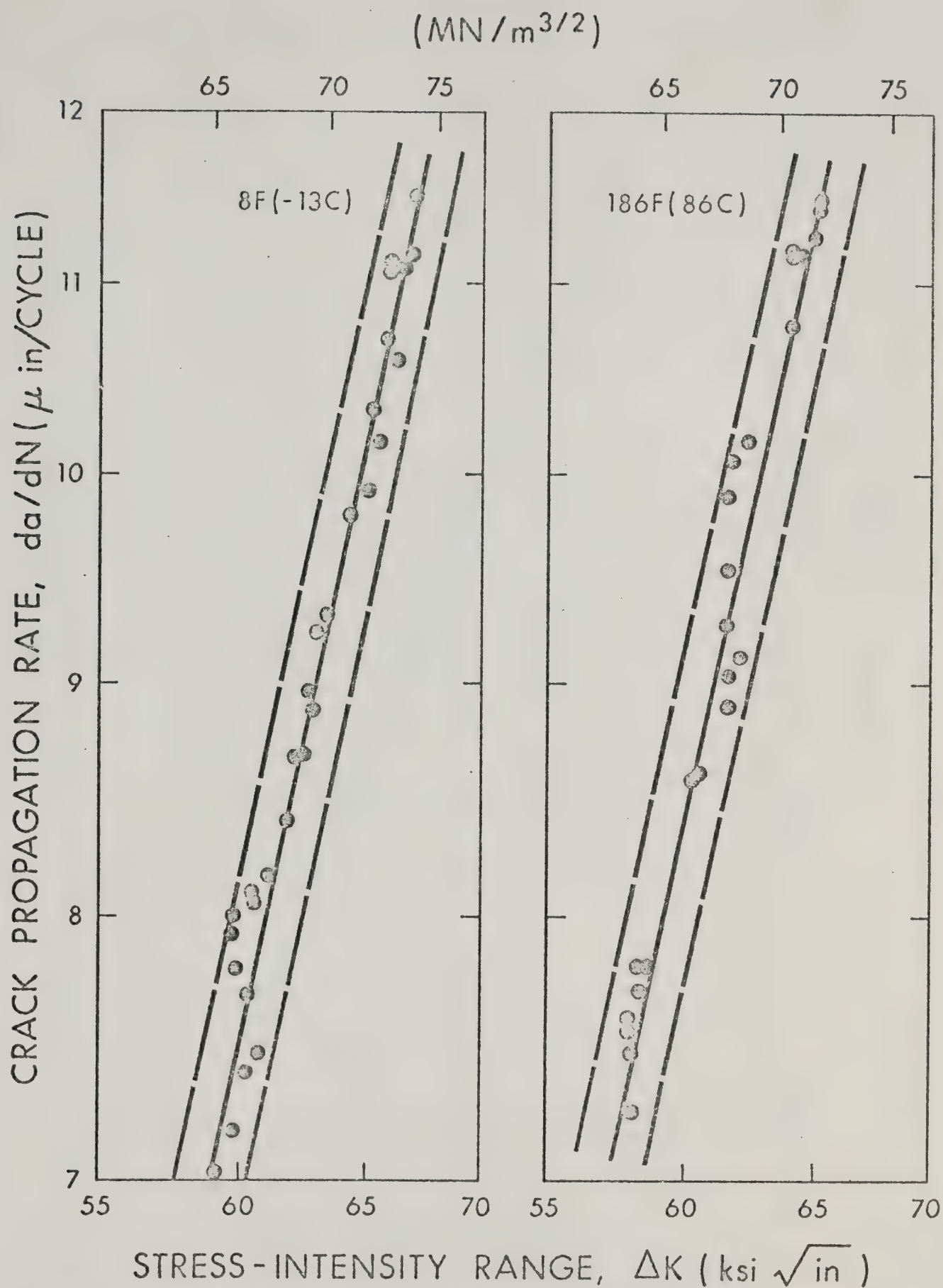


FIGURE 17: Crack propagation rate as a function of stress-intensity range for the H.A.Z. at -13°C and 86°C

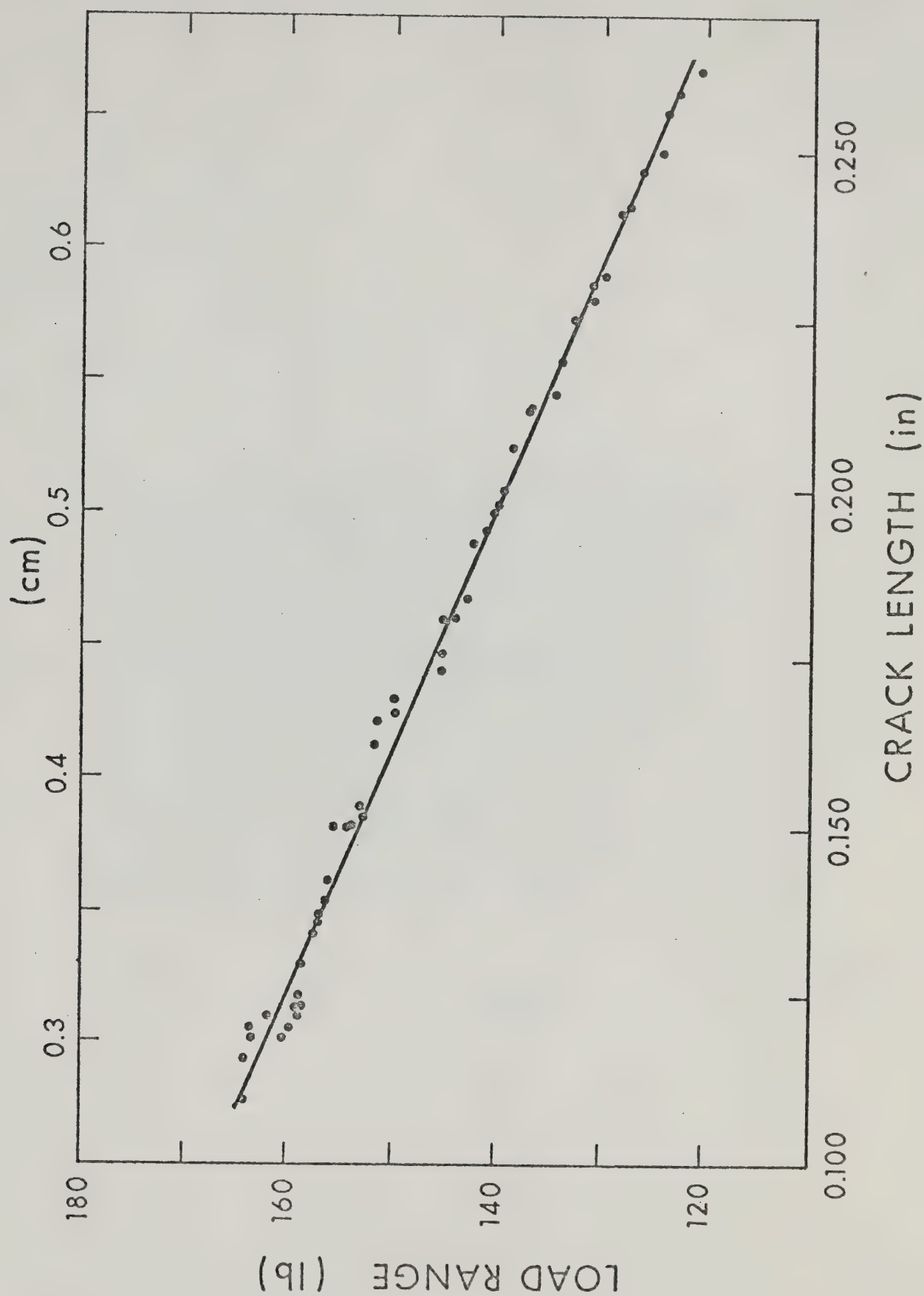


FIGURE 18: Load range versus crack length for a 21C base metal test



FIGURE 19: Irregular crack propagation in the -13C H.A.Z. test
(X500)

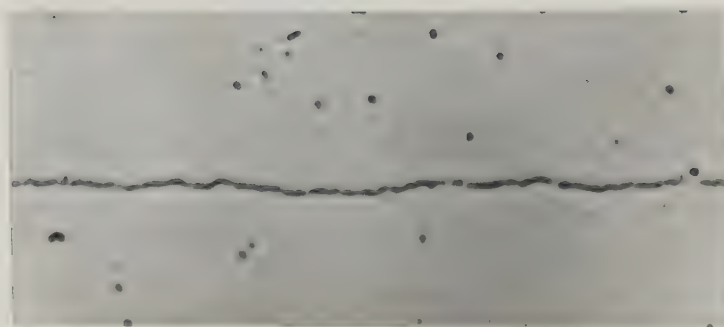


FIGURE 20: Planar crack propagation for a 21C base metal test
(X100)

FIGURE 21: Crack growth rate for $\Delta K = 63 \text{ ksi}\sqrt{\text{in}}$,
as a function of temperature

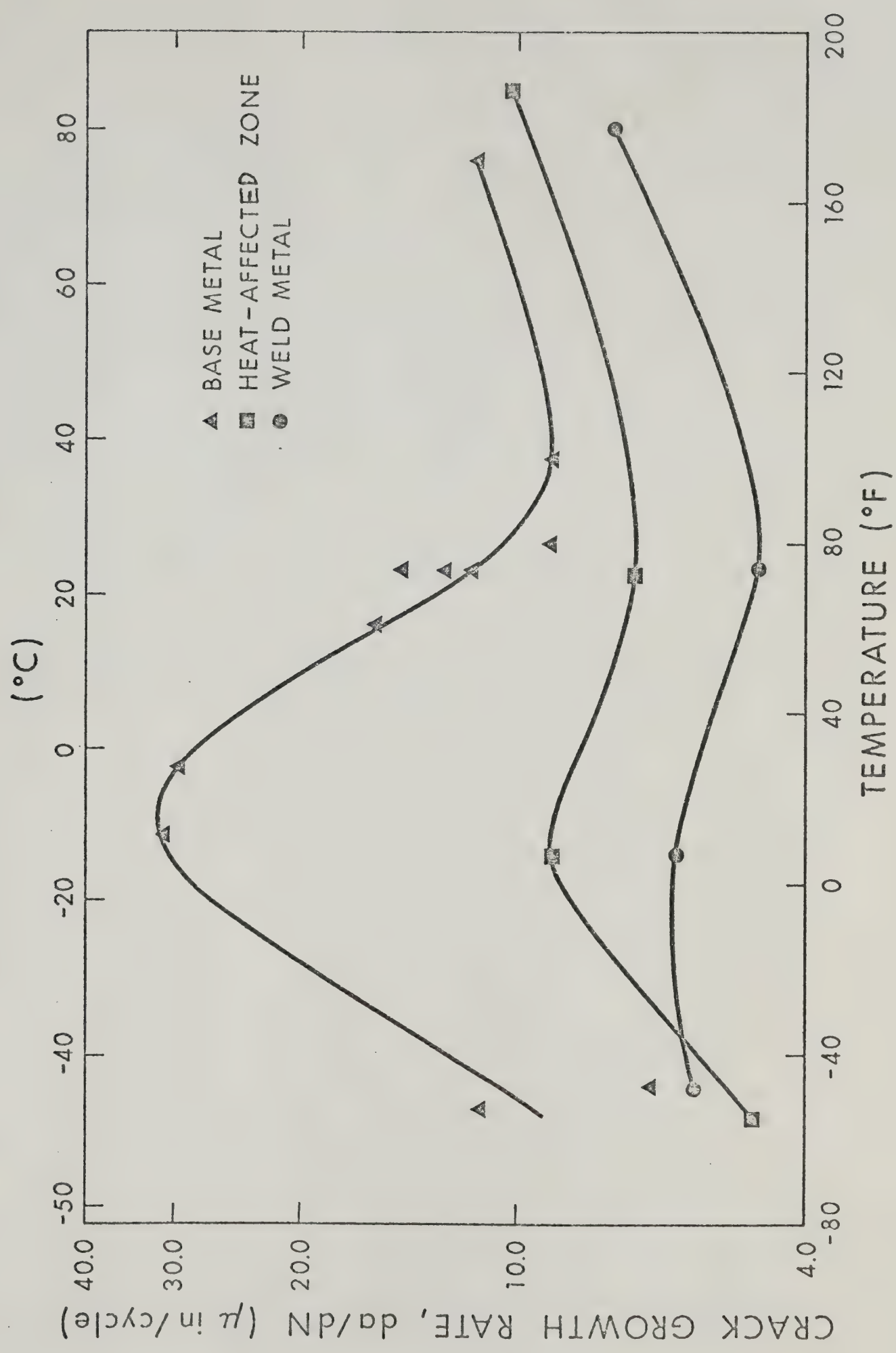


FIGURE 22: Stress-intensity range for $da/dN = 8.9$ micro-inch/cycle,
as a function of temperature

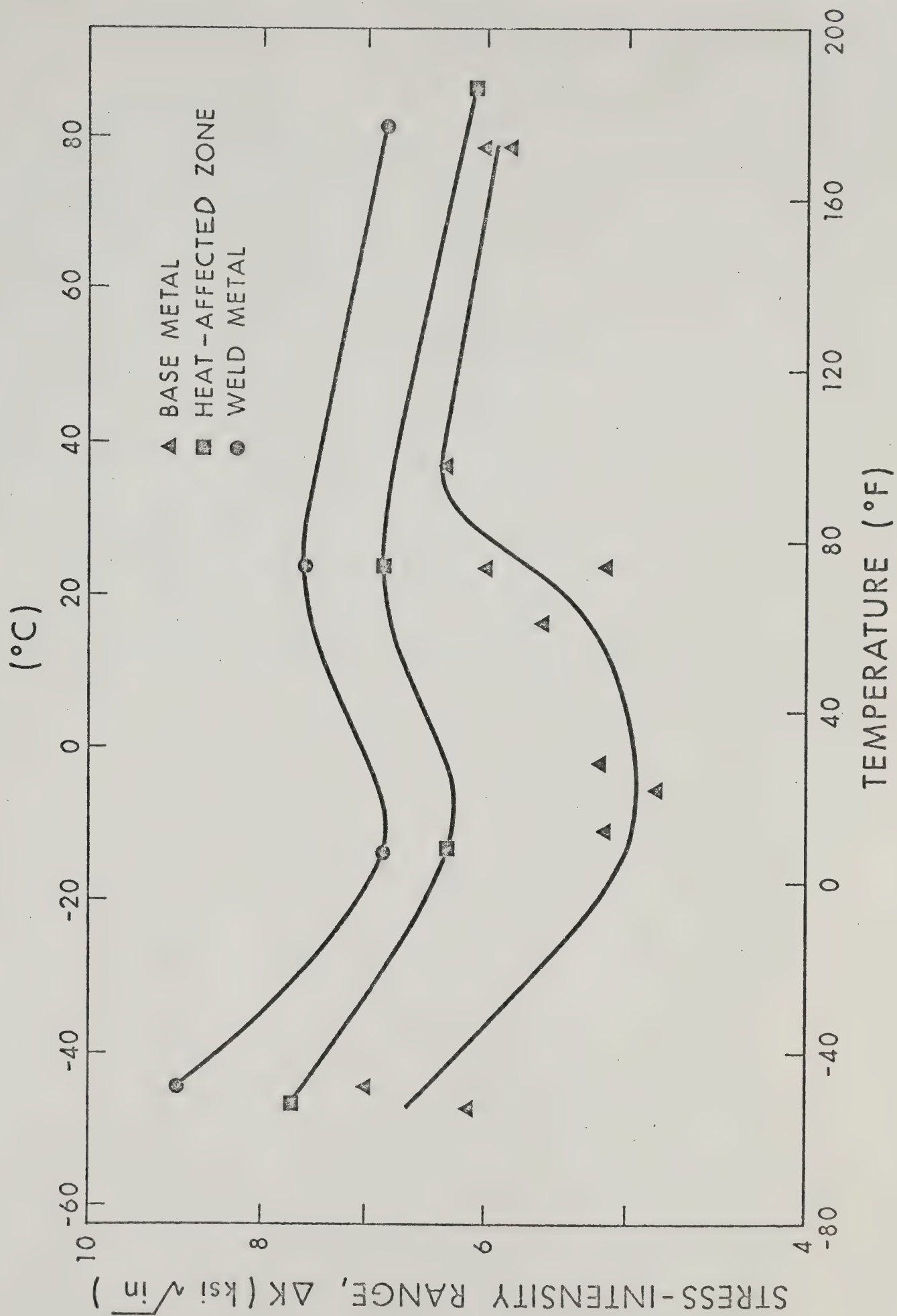
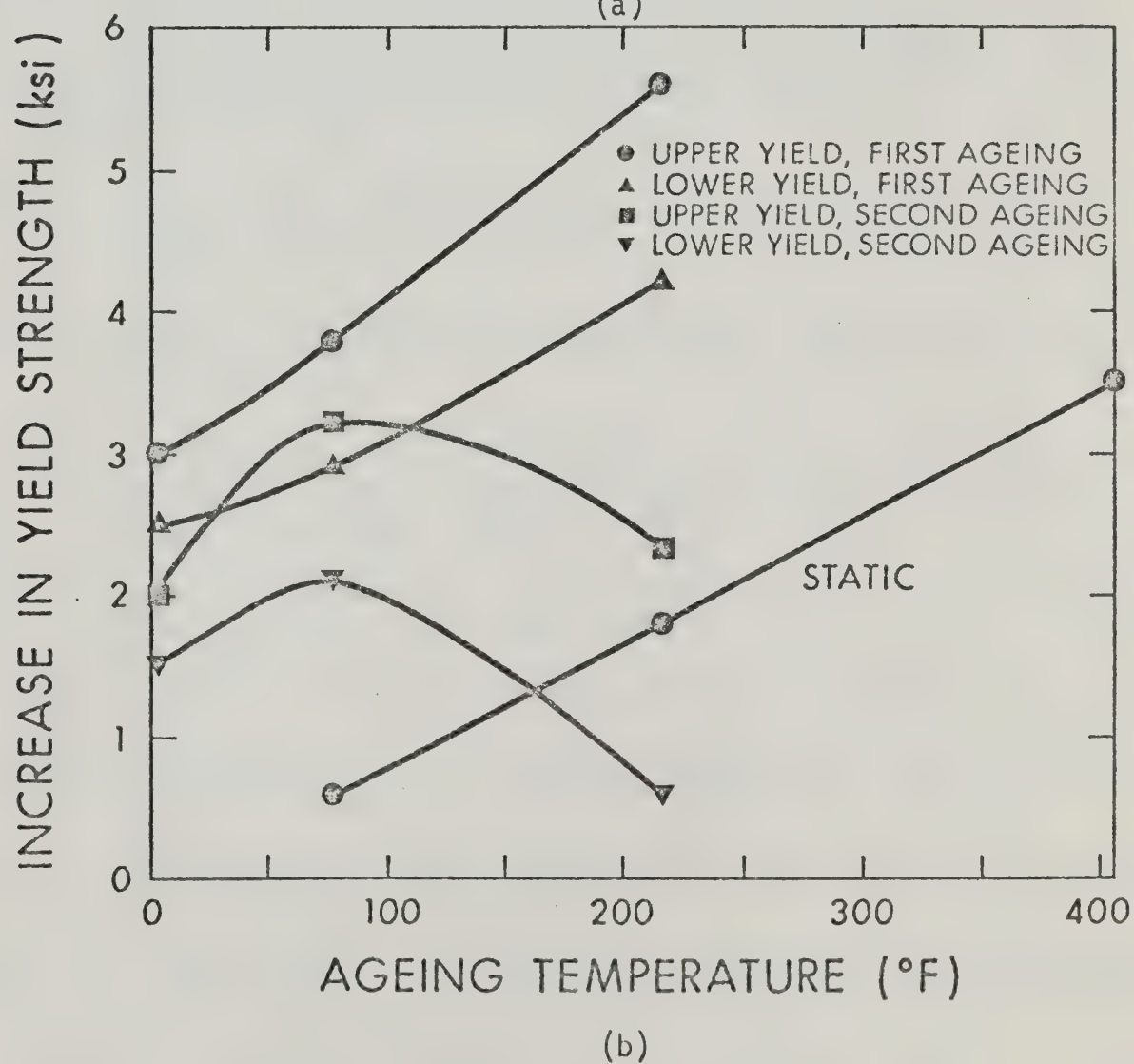
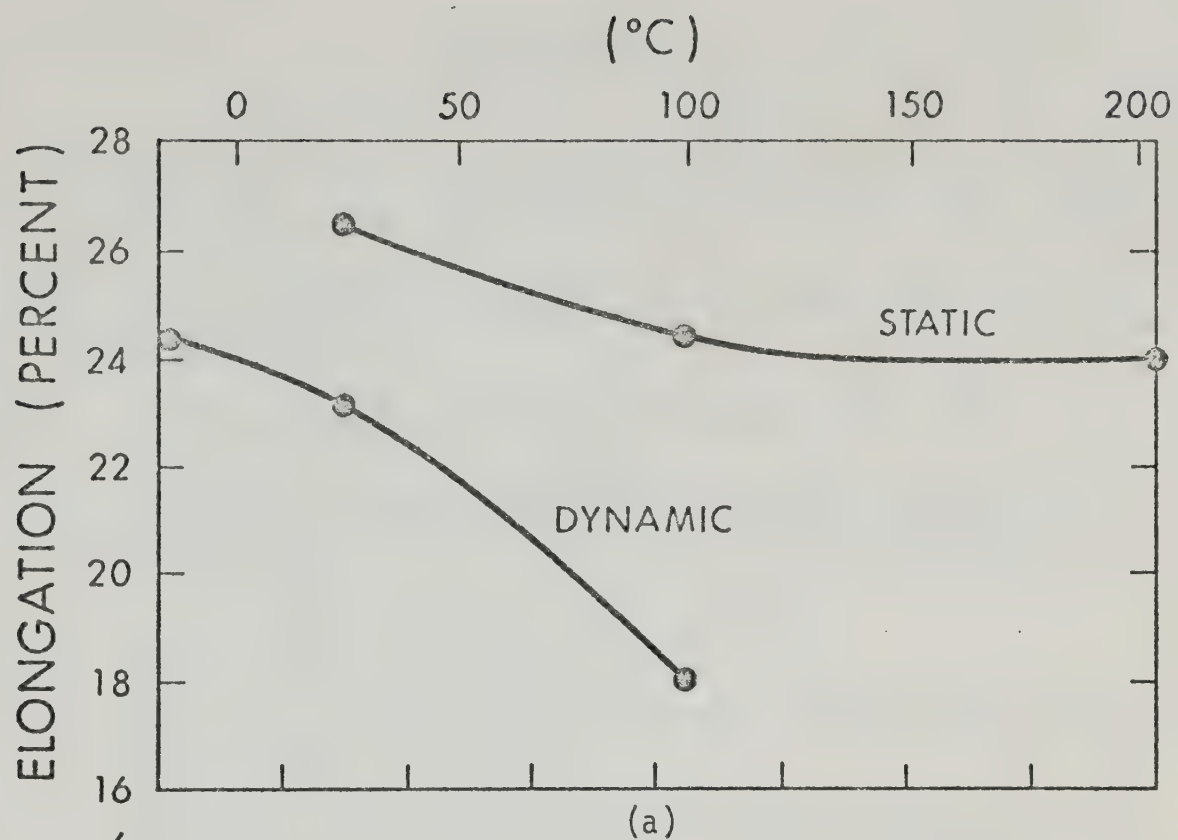


FIGURE 23: Results of one-hour static or cyclic strain-ageing on room temperature properties:

- (a) total elongation as a function of ageing temperature
- (b) increases in yield strengths as a function of ageing temperature



BIBLIOGRAPHY

- Adair, A., and H. Lipsitt, On the Fatigue-Limit Behaviour of Iron and Mild Steel, Trans. Met. Soc. AIME, 236, 1235 - 1237, 1966.
- Andreasen, D., Fatigue Crack Propagation in Pipeline Steel, Masters Thesis, Department of Mining and Metallurgy, University of Alberta, 1973.
- Baird, J., Iron and Steel, 36, 186, 326, 368, 400, 450, 1963.
- The Effects of Strain-ageing due to Interstitial Solutes on the Mechanical Properties of Metals, Metals and Materials, 5, 1 - 18, 1971.
- Barnby, T., J. Iron and Steel Inst., 204, 23, 1966.
- Bilby, B., and P. Heald, Crack Growth in Notch Fatigue, Proc. Roy. Soc. (London), A305, 429, 1968.
- Bucci, R., Clark, W., and P. Paris, Fatigue Crack Propagation Rates Under a Wide Variation of ΔK for an ASTM A517 Grade F (T-1) Steel, Stress Analysis and Growth of Cracks, ASTM STP 513, 177 - 195, 1972.
- Clark, W., Fatigue Crack Growth Characteristics of ASTM A533 Grade B Class 1 Steel Base Plate Weld Metal and Heat Affect Zone, Westinghouse Research Report 69 - 7E7 - BFPWR - R2, 1969.
- Dolby, R., Fracture Toughness Comparison of Weld H.A.Z. and Thermally Simulated Microstructures, Metal Const. and Br. Weld. J., 4, No. 2, 59, 1972.
- Donahue, R., Clark, H., Atanmo, P., Krumble, R., and A. McEvily, Crack Opening Displacement and the Rate of Fatigue Crack Growth, Int. J. Frac. Mech., 8, No. 2, 209 - 219, 1972.
- Doremus, R., The Precipitation of Carbon from Alpha Iron: II. Kinetics, Trans. AIME, 218, 596 - 605, 1960.
- Fast, J., Interaction of Metals and Gases, Volume 2, Academic Press, 1965.
- Fisher, J., Fatigue Strength of Welded A514 Steel Beams, Proc. Fatigue of Welded Structures, 1, 135 - 148, 1970.
- Ford, G., Application of Fracture Mechanics to Pipe Line Design, J. Eng. Inst. of Canada, 1972.
- Forrest, P., Speed Effects in Fatigue, Proc. Roy. Soc., A242, 223, 1957.

- Gentilicore, V., Pense, A., and R. Stout, Fracture Toughness of Pressure Vessel Steel Weldments, Weld. J. Suppl., 49, No. 8, 341 - 353, 1970.
- Gurney, T., (a) Fatigue of Welded Structures, Cambridge Press, 1968.
- (b) An Investigation of the Rate of Propagation of Fatigue Cracks in the Range of Steels, Weld. Inst. Report E18/12/68, December, 1968.
- Hall, E., Yield Point Phenomena in Metals and Alloys, Macmillan, 1970.
- Harrison, J., The Analysis of Fatigue Test Results for Butt Welds with Lack of Penetration Defects Using a Fracture Mechanics Approach, Proc. 2nd. Int. Conf. in Fracture, Brighton, 1969, Chapman and Hall, 1969.
- Head, A., The Propagation of Fatigue Cracks, J. Applied Mech., 23, 407 - 410, 1956.
- Hundy, B., and T. Boxall, The Repeated Strain Ageing of Mild Steel, Metallurgia, 55, 27 - 30, January, 1957.
- Kenyon, N., Morrison, W., and A. Quarrell, The Fatigue Strength of Welded Joints in Structural Steels, Br. Weld. J., 13, No. 3, 123 - 137, 1966.
- Kies, J., Smith, H., Romine, H., and H. Bernstein, Fracture Testing of Weldments, in Fracture Toughness Testing, ASTM STP 381, 1965.
- Lardner, P., A Dislocation Model for Fatigue Crack Growth in Metals, Phil. Mag., 17, 71, 1968.
- Levy, J., Strain-Ageing as an Explanation of the 'Knee' in the Fatigue Curve for Mild Steel, Acta. Met., 56, 71 - 73, 1957.
- Levy, J., and G. Sinclair, An Investigation of Strain Ageing in Fatigue, ASTM Proc., 55, 866, 1955.
- Liu, H., Crack Propagation in Thin Metal Sheets Under Repeated Loading, Trans. ASME, 83, 23 - 31, 1961.
- Maddox, S., Fatigue Crack Propagation in Weld Metal and Heat-affected Zone Material, Weld. Inst. Report E/29/69, December, 1969.
- McClintock, F., On the Plasticity of the Growth of Fatigue Cracks, Fracture of Solids, Wiley, 1963.
- McEvily, A., and T. Johnson, On the Role of Cross-Slip in Brittle Fracture and Fatigue, Int. Conf. on Fracture, Sendai, Japan, 1965.

- Mintz, B., and D. Wilson, Strain Ageing During the Fatigue of Carbon Steels, Acta. Met., 13, 947 - 956, 1965.
- Modlen, G., and G. Smith, J. Iron and Steel Inst., 154 - 159, Feb., 1960.
- Munse, W., Fatigue of Welded Structures, Welding Research Council, 1964.
- Nibbering, J., and A. Lalleman, Low Cycle Fatigue Problems in Shipbuilding; crack Propagation in Coarse-Grained Zone of Thick Plates, Proc. Fatigue of Welded Structures, 1, 257 - 272, 1970.
- Oates, G., and D. Wilson, The Effects of Dislocation Locking and Strain Ageing on the Fatigue Limit of Low-Carbon Steel, Acta. Met., 12, 21 - 33, 1964.
- Paris, P., The Fracture Mechanics Approach to Fatigue, Proc. Tenth Sagamore Army Materials Research Conference, 1963, 107 - 132,
- Riccardella, P., and T. Mager, Fatigue Crack Growth Analysis of Pressurized Water Reactor Vessels, ASTM STP 513, 260 - 279, 1972.
- Rice, J., Plastic Yielding at a Crack Tip, Proc. Int. Conf. Fracture, Sendai, Japan, 1965.
- Mechanisms of Crack Tip Deformation and Extension by Fatigue, Fatigue Crack Propagation, ASTM STP 415, 247, 1967.
- Tall, L., Initial Findings from a Study in Low Cycle Fatigue of Welded ASTM A514 Steel, Proc. Fatigue of Welded Structures, 1, 208 - 217, 1970.
- Thompson, N., and N. Wadsworth, Metal Fatigue, Advances in Phys., 7, 72 - 169, 1958.
- Tompkins, B., Fatigue Crack Propagation -- An Analysis, Phil. Mag., 18, 1041 - 1066, 1968.
- Weibull, W., Theory of Fatigue Crack Propagation in Sheet Specimens, Acta. Met., 11, 745 - 752, 1963.
- Wessel, E., Linear Elastic Fracture Mechanics for Thick-walled Steel Pressure Vessels: material property considerations, Symposium on Fracture Toughness Concepts for Weldable Structural Steels, UKAEA, Cultheth, England, Chapman and Hall, 1969.

B30082